A refinement of coccolith separation methods: Measuring the sinking characters of coccoliths

Hongrui Zhang[1, 2], Heather Stoll[2], Clara Bolton[3], Xiaobo Jin[1], Chuanlian Liu[1]

[1] State Key Laboratory of Marine Geology, Tongji University, Shanghai, 200092, China

[2] Geological Institute, Department of Earth Science, Sonneggstrasse 5, ETH, 8092, Zürich, Switzerland

[3] Aix-Marseille Univ, CNRS, IRD, Coll de France, CEREGE, Aix en Provence, France.

Correspondence to: Chuanlian Liu (liucl@tongji.edu.cn)

Abstract. Quantification sinking velocities of individual coccoliths will contribute to optimizing laboratory methods for separating coccoliths of different sizes and species for geochemical analysis. The repeat settling/decanting method was the earliest method proposed to separate coccoliths from sediments, and is still widely used. However, in the absence of estimates of settling velocity for non-spherical coccoliths, previous implementations have depended mainly on time consuming empirical method development by trial and error. In this study, the sinking velocities of coccoliths belonging to different species were carefully measured in a series of settling experiments for the first time. Settling velocities of modern coccoliths range from 0.154 to 10.67 cm h^{-1}. We found that a quadratic relationship between coccolith length and sinking velocity fits well and coccolith sinking velocity can be estimated by measuring the coccolith length and using the length-velocity factor, k_v. We found a negligible difference in sinking velocities measured in different vessels. However, an appropriate choice of vessel must be made to avoid 'hindered settling' in coccolith separations. The experimental data and theoretical calculations presented here support and improve the repeat settling/decanting method.

1. Introduction

Coccolithophores are some of the most important phytoplankton in the ocean. They can secrete calcareous plates called coccoliths, which contribute significantly to discrete particulate inorganic carbon in the euphotic zone and to $CaCO_3$ fluxes to the deep ocean (e.g., Young and Ziveri, 2000; Sprengel et al., 2002). Coccolith morphyology, geochemisity and fossile assemblage composition can reflect paleoenvironmental changes (e.g., Beaufort et al., 1997; Stoll et al., 2002; Zhang et al., 2016). However, the use of coccolith geochemical analyses in paleoenvironmental reconstructions was so far hindered by the difficulty of isolating coccolith compared with foraminifera. Two main methods have been developed to concentrate near-monospecific assemblages of coccoliths from bulk sediments: one is the method based on a decanting technique (Paull and Thierstein, 1987; Stoll and Ziveri, 2002) and the other is that based on microfiltration (Minoletti et al., 2009). The improvement of separation techniques offered a new perspective to study the Earth's history (e.g. Stoll, 2005; Beltran et al., 2007; Bolton and Stoll, 2013; Rousselle et al., 2013). Moreover, the development of coccolith oxygen and carbon isotope studies in culture in recent years (e.g. Ziveri et al., 2003; Rickaby et al., 2010; Hermoso et al., 2016; McClelland et al., 2017) has provided an improved mechanistic understanding of coccolith isotope data and therefore stimulated the need for more purified coccolith fraction samples from the fossil record.

Both decanting and microfiltering are widely used methods for coccolith separation. The microfiltering method separates coccoliths with polycarbonate mirco-filter membrane (with pore sizes of 2μm, 3μm, 5μm 8μm, 10μm and 12μm). This method is highly effective in the larger size ranges, but is very time consuming in sediments with a high proportion of small (<5μm) coccoliths (which tends to be the case in natural populations). It is also impossible to separate coccoliths with similar lengths by microfiltration, such as *Florisphaera profunda* and *Emiliania huxleyi* (Hermoso et al., 2015). Decanting, on the other hand, is highly effective for the small-sized coccoliths, because their slow settling times permit a greater ability to separate different sizes. Consequently, in some studies, a combination of the micro filtering and sinking or centrifugation method were applied for coccolith separation (Stoll, 2005; Bolton et al., 2012; Hermoso et al., 2015). The repeated sinking/decanting method, first employed by (Edwards, 1963; Paull and Thierstein, 1987) follows the simple principle formalized by Stokes' Law for spherical particles: particles of larger size settle

more quickly because they have a higher ratio of volume and mass (accelerating sinking) to sectional area (resistance retarding sinking). However, the sinking velocities of coccoliths with complex shape are difficult to calculate and have not been quantified in previous studies. Consequently, the repeated decanting method has generally used settling times based on empirical trial and error.

In the current study, we present a novel and rigorous estimation of sinking velocity for 16 species of modern and Cenozoic coccoliths, carefully measured in 0.2% ammonia at 20℃. With this new dataset, we explore how to estimate the sinking velocity of coccoliths based on their shape and length, which allows our estimations to be generalized for other species, and for situations where the mean length of coccoliths of a given species was different from that of our study. These generalizations, together with our results on sinking velocities of one coccolith species (*Gephyrocapsa oceanica*) in different vessels, should allow a significant improvement in efficiency of future protocols for separation of coccoliths by repeated decanting.

2. Materials and methods

2.1 Sample selections

We measured the sinking velocity of 16 different species of coccoliths, isolated from eight deep-sea sediment samples from the Pacific and Atlantic Oceans (Figure 1, Table A1). Sample were principally of Quaternary age but include two Neogene/Paleogene samples. In general, numbers of small coccoliths, including *E. huxleyi*, *Gephyrocapsa* spp and *Reticulofenestra* spp. are about an order of magnitude greater than that of larger coccoliths. However, the larger coccoliths' contributions to carbonate can be as high as 50% (Baumann, 2004; Jin et al., 2016). Moreover, both small coccoliths and large coccoliths are useful in geochemical analyses (Ziveri et al., 2003; Rickaby et al., 2010; Candelier et al., 2013; Bolton et al., 2012, 2016; Bolton and Stoll, 2013). Therefore, both small and large coccoliths were studied in this research. (B). Pictures of the studied coccolith are shown in Appendix B, and all classifications follow Nannotax3 except *Reticulofenestra* spp. (Figure C2 in Appendix C).

2.2 Experiment designs

2.2.1 Sample pretreatments

The sinking velocity measurement depends on absolute abundance estimation (more details in 2.2.2).

However, on microscope slides, larger coccoliths and foraminifer fragments may cover smaller coccoliths, reducing the accuracy of coccolith absolute numbers. Thus, before sinking experiments were carried out, raw sediments were pretreated to purify the target coccoliths to reduce errors in coccolith counting. The raw sediments were disaggregated in 0.2% ammonia and sieved through a 63 μm sieve and then treated by sinking method or filtering method (Bolton et al., 2012; Minoletti et al., 2009) to concentrate the target species up to at least more than 50% of the total assemblage (for Noëlaerhabdaceae coccoliths, a percentage more than 90% can be easily achieved). In one sample with aggregation (ODP 807), we did a rapid settling (30 min, 2 cm) to eliminate aggregates. Most of the species were measured individually in settling experiments, except for *Pseudoemiliania lacunosa* and *Umbilicosphaera sibogae*, which were measured together.

2.2.2 Measuring the sinking speeds of coccoliths

We are not aware of any prior direct determination of the sinking velocity of individual coccoliths, although the sinking velocities of live coccolithophores and other marine algal cells have been successfully measured by the 'FlowCAM' method (Bach et al., 2012) or a similar photography technique (e.g. Miklasz and Denny, 2010). Here we introduce a simple method to measure the particle sinking speeds without special equipment.

1. After pretreatment, the coccolith suspensions were gently shaken and then moved into comparison tubes which were vertically mounted on tube shelves. We set the timer going and let the suspension settle for a specified period of time, marked as sinking time or settling duration (T);
2. Thereafter, we removed the upper 15 ml supernatant into a 50 ml centrifuge tube with a 10 ml pipette. This operation was performed slowly and gently to avoid drawing lower suspensions upward. The absolute counting of cocolith was achieved by using the 'drop technique' to make quantitative microscope sides (Koch and Young, 2007; Bordiga et al., 2015). 0.3 ml mixed suspension was extracted and pipettes onto a glass cover and dry the slider on a hotplate;
3. The lower suspension was than to homogenized and another slider was prepare as described above;
4. The number of coccoliths in the upper and lower suspensions were carefully counted on

microscope at ×1250 magnification and the number of coccoliths and fields of view (FOV) were recorded for further calculations. More than 300 specimens were counted for most of the measurements. For the *Helicosphaera carteri* measurements, more than 100 FOV were checked and about 100 specimens were counted.

To calculate the sinking velocities of coccoliths, we define a parameter named the separation ratio (R), which represents the percentage of removed coccoliths in one separation by pumping out the upper suspension. This parameter is important and will be repeatedly mentioned in the following part. R was measured using the following equation (more details about derivation can be found in Appendix D):

$$R = \frac{\frac{N1}{n1} \times V_1}{\frac{N1}{n1} \times V_1 + \frac{N2}{n2} \times V_2} \quad (2\text{-}1)$$

where N_1 and N_2 are numbers of coccoliths counted in upper and lower suspension slides, respectively; n_1 and n_2 are the number of FOV counted. V_1 and V_2 are the volume of the settling vessel defined by the settling distance, as shown in Figure 2.

The separation ratio, R, also has a relationship with sinking time, T (Appendix D):

$$R = \frac{V_1 - \frac{V_1}{D} \times v \times T}{V_1 + V_2} \quad (2\text{-}2)$$

where V_1, V_2 and D are shape parameters shown in Figure 2; and v is the average sinking velocity of measured coccoliths. If we plot R against T, the slope of line has a relationship with v. Then liner regressions between R and T were processed with MATLAB to calculate the v (details about error analyses can be found in Appendix E).

There are still two issues to be explained. Firstly, to eliminate the shape differences among vessels, all separation ratios have been transferred to calibrated separation ratios (R_{cal}), which means the separation ratio measured in a standard vessel with V_1=15 ml, V_2=10 ml and D=6 cm (more details about transformation from R to R_{cal} can be found in Appendix D). Secondly, we treated the average sinking velocities as the sinking velocities of the coccoliths with the average length. This approximation has been proved reasonable in Appendix D.

2.2.3 Detecting the potential influence of vessels

Seven commonly used vessels were selected to detect the potential influence of vessels (Figure 3). Two of them are made of plastics (No.2 and No.3 in Figure 3) and all others are pyrex glass vessels. About 500 mg of sediment from core KX21-2 were pretreated as described in 2.2.1 and suspended

in about 500 ml ammonia. After that, settling experiments were performed as described in 2.2.2 using different vessels. In these experiments, only the dominant species, *G. oceanica*, was measured.

2.2.4 Other factors influencing the sinking velocity

Temperature can change the density and viscosity of liquid. Generally speaking, the higher the temperature is, the lower the density and viscosity will become and the faster pellets will sink. Take water for instance, if the temperature increases from 15 to 30℃, the particle sinking velocity will increase by ~43% (Table 1). All sinking velocities measured or discussed in the following sections were velocities at 20℃ to minimize the influence of temperature.

The calibration of sinking velocity in high concentration suspension has been calculated by Richardson and Zaki (1954)

$$v = v_0(1 - \alpha_s)^{2.7} \quad (2\text{-}3)$$

where the α_s is the solids volume fraction. Based on equation 2-3, the higher the suspension concentration is, the slower the sinking velocity will be. That is so called 'hindered settling'. When the α_s=0.2%, the reduction of sinking velocity owing to hindered settling is negligible (v/v_0 equals 99.46%). Hence, in this study all suspensions have solid volume fractions lower than 0.2% to avoid notable reductions of coccolith sinking velocities.

3. Results and Discussions

3.1 Influence of vessels

The sinking velocities of *G. oceanica* in the core KX21-2 in 0.2% ammonia at 20℃ measured in different vessels vary from 0.99 to 1.23 cm h^{-1}. The lowest value occurred in the 100 ml centrifuge tube and the highest sinking velocity was measured in the 50 ml centrifuge tube experiments. The correlations between sinking velocities and different vessel parameters are quite low: r=0.13 for the vessel inner diameter, r=0.0005 for the sinking distance and r=0.051 for the upper volume and total volume ratio ($V_1/(V_1+V_2)$). The dissipation of energy by friction between the moving fluid and the walls can cause a reduction of sinking speed (wall effect). A significant wall effect will be detected when a particle is settling in a vessel with a diameter that is smaller than the particle size by two orders of magnitude (Barnea and Mizarchi, 1973). The length of coccoliths is on the micron scales, so the diameters of vessel used in laboratory are more than four orders of magnitude larger than

coccoliths. Moreover, our results show that the difference between vessel materials, glass and plastics, can also be ignored (Figure 4). Hence, we suggest that vessel type almost has no significant influence on sinking velocity of coccoliths.

However, our experiments were premised on the basis that the concentration of suspension was equal among different vessels. This means that large vessels can treat more sediment at one time but if we choose a larger vessel, more suspensions should be pumped and it often costs more time in sinking (often due to longer sinking distance). Assuming that the sediment is composed of 50% calcite (with density of 2.7 g cm^{-3}) and 50% clay (about 1.7 g cm^{-3}), the largest amount of sediment that can be used without significant reduction of the sinking velocity (5%) is about 400 mg in 100 ml suspension (this calculation is based on equation 2-3). However, because sediments accumulate in the lower suspension, the particle concentration can be more than 4 times higher than in the initial homogenous concentration. This phenomenon will be more significant for a vessel with a narrow bottom, such as centrifuge tubes. To avoid this, we recommend using about 100 mg dry sediment suspended in at least 100 ml suspension to avoid 'hindered settling'. If more sediment is necessary for geochemistry analyses, then a larger vessel should be selected to separate enough sample at one time.

3.2 Sinking velocities at 20℃ in 0.2% ammonia

We measured the separation ratios of different coccoliths in comparison tubes at 20℃ in 0.2% ammonia (Figure 5). The sinking velocities of coccoliths were then calculated by linear fitting of separation ratios and settling durations. The sinking velocities of studied coccoliths vary by two orders of magnitude from 0.154 cm h^{-1} to 10.67 cm h^{-1} (Table 2). The highest sinking velocity was found in the measurement of *Coccolithus pelagicus* and the lowest velocity was found for *F. profunda*. The average sinking speed of coccoliths is about 10-50% of the terminal sinking velocities of calcite spheres calculated by Stokes' Law (Figure 6c). These ratios are comparable to the oval objects (e.g. seeds) data from Xie and Zhang (2001) and smaller than steel ellipsoids data from McNown and Malaika (1950). The sinking velocities of coccoliths measured in our experiment are about 2-3 orders of magnitude smaller than values from sediment traps of 143-243 m d^{-1} (595~1012 cm h^{-1}) in the North Atlantic (Ziveri et al., 2000 and Stoll et al., 2007), suggesting that the coccoliths sinking out of the euphotic layer are mainly in the form of sinking aggregates rather than individual

194 coccoliths.

195 **3.3 Estimating the sinking velocities**

196 Generally speaking, the sinking velocities of coccoliths increase with distal shield length (Figure
197 5a), as expected from the increase in volume to sectional area for a given geometry as length
198 increases. Our data implies that the sinking velocity has a power function relationship with distal
199 shield length.

200 We propose that the sinking velocity of coccoliths might have a quadratic relationship with distal
201 shield length as described by Stokes' Law (Figure 6a). If we use data for all species except *H. carteri*
202 (the reason can be found in the following discussion), the sinking velocities can be described by the
203 following equation:

204 $$v = 0.0982\ (\pm 0.001) * \phi^2 \quad (3\text{-}1)$$

205 Based on this quadratic regression, we derive a shape-velocity factor (k_v) that relates settling
206 velocity to coccolith length.

207 $$v = k_v * \phi^2 \quad (3\text{-}2)$$

208 Furthermore, this factor is analogous to the shape-mass factor, 'k_s' used to relate coccolith mass to
209 coccolith length (Young and Ziveri, 2000). The length and shape-velocity factor of coccoliths can
210 be used to predict most of the sinking velocity variations, however, variations may also arise due to
211 changes in coccolith mass and thickness, for a given length, and due to the hydrodynamics of
212 particular shapes. We noticed that the smaller coccolith *G. caribbeanica* has a greater sinking
213 velocity than the larger coccolith, *G. oceanica*. We suggest that this was caused by greater mass per
214 length (or greater average thickness) in the case of *G. caribbeanica* and this may be due to the closed
215 central area while *G. oceanica* has an open central area. Another example is *H. carteri*, which lower
216 sinking velocity of which can be explained by the unique structure of *H. carteri* coccolith . Firstly,
217 the broad edge of *H. carteri* can increase the drag force significantly. . Moreover, most of the
218 measured coccoliths have a ellipticity (major axis length and minor axis length ratio) larger than 0.8,
219 while the ellipticity of *H. carteri* is around 0.6, which means the mass of *H. carteri* is smaller than
220 other species of coccoliths with similar lengths (Figure 6d and Figure C3). That is also the reason
221 *H. carteri* was excluded from the general regression in equation 3-1. In the case of partial dissolution,
222 the well-preserved *Cyclicargolithus floridanus* may have higher mass than dissolved (or

disarticulated) *Cy. floridanus*, and therefore a slightly higher shape-velocity factor.

4. Suggestions for coccolith velocity estimations and separations

To improve coccolith separation by settling methods, we measured sinking velocities of different coccoliths by gravity. Sinking velocities in this study varied from 0.154 to 10.61 cm h^{-1}, about 10% to 50% of those of calcite spheres with same diameter. The shape of different vessels had little impact on the sinking velocity. But we should consider the volume of vessels to avoid 'hindered settling'. The sinking velocities are mainly controlled by the shape of coccolith, including the distal shield length, the size of central area, and the ellipticity of coccoliths. Besides the shape of coccoliths, temperature is also crucial to the coccolith separations because of the dependence of sinking velocities on temperature. Length-velocity factors were proposed to estimate coccoliths sinking velocities, so coccolith separation can be achieved by following steps:

1. Measure the length of coccoliths in your target assemblage under the microscope and regress the length distribution by the assumption of normal distribution (details are in Appendix C);
2. Estimate sinking velocities for each important species. For species which sinking speed has been directly measured, we can use the length-velocity factor directly ($v=k_v * \phi^2$). For unmeasured species, we can choose the length-velocity factor of coccoliths with similar morphology in this study or use the general length-velocity formula ($v=0.098(\pm 0.001) * \phi^2$);
3. Calculate the separation time for main species. For example, in KX21-2 there are three main coccoliths, *F. prounda*, *G. oceanica* and *Ca. leptoporus* and we wish to separate *G. oceanica* out from the bulk sediment. Calculate each cococliths' sinking velocity distributions as described in Step 2 above. As shown in Figure 7, a sinking velocity intermediate between *F. profunda* (with a length 2σ larger than average, marked as +2σ) and G. oceanica (with a length 2σ smaller than average, marked as -2σ) optimal to separate them, would be 0.6 cm h^{-1}. Similarly, we can chose speed thresholds 1.85 cm h^{-1} to separate *G. oceanica* from *Ca. leptoporus*. If we settle in a 50 ml centrifuge tube with a sinking distance, D, equal to 5.84 cm, the sinking time for separating *F. profunda* should be T=5.84/0.6=9.73 h. Similarly, we can calculate the time for separating *G.*

oceania by T=5.84/1.85=3.16 h;

4. Homogenize the sediment suspension and let coccoliths settling as the period calculated in Step 3. After that, pump out the upper part of suspension. In the upper part, we have exclusively the smaller of the main coccoliths. However, column will still contain some smaller ones. So this step (settling and pumping) should be repeated until the lower part no longer has significant contribution from the smaller coccoliths. This step has been well described in pervious studies and more details can be found in Stoll and Ziveri (2002) and Bolton et al. (2012).

We find, if we use the general formula, a closed central area coccolith will sink faster than prediction (for *G. caribbeanica* and small *Ca. leptoporus* will settle ~40% faster) and coccoliths with greater ellipticity can settle much slower (for *H. carteri* will settle as 30% of the predicted sinking velocity for coccolith with similar length). Moreover, the sinking method cannot separate every species of coccoliths perfectly. As mentioned in Section 2.2.1, *P. lacunosa* and *U. sibogae* cannot easily be separated from each other because they have similar sinking velocities. Nevertheless, this study provides the first direct estimation of coccolith settling velocities, which should simplify implementation of future methods to separate coccoliths by settling time.

Acknowledgements. This study was supported by grants from the Chinese National Science Foundation (91428310, 91428309 and 41530964, to L.C.). We thank the Integrated Ocean Drilling Program (IODP) for providing the samples. The IODP is sponsored by the U.S. National Science Foundation and participating countries under management of the IODP Management International, Inc (IODP-MI).

Table 1. The influence of temperature on sinking velocity. Density data is from Kell (1975) and viscosity data is from Joseph et al. (1978).

T (℃)	ρ (g cm^{-3})	η (mPa s)	$v_T : v_{T=20}$
15	0.9991	1.1447	0.8804
20	0.9982	1.0087	1
25	0.9970	0.8949	1.1279
30	0.9956	0.8000	1.2627

Table 2. The sinking velocity and shape-velocity factor of different coccolith species: ϕ means the distal shield length of coccolith and St ϕ is the standard deviation of distal shield length; sv represents the sinking velocity; v (95%-) and v (95%+) represent the lower and higher limit of 95% confidence level, respectively. 'k_v' represents the length-sinking velocity factor. The short name of coccolith can be found in the caption of Figure 4. The details of coccoliths length distribution are in Appendix C.

Species	**abb.**	**ϕ (μm)**	**St ϕ (μm)**	**sinking velocity (cm h^{-1})**	**v (95% -)**	**v (95% +)**	**k_v**
F. profunda	Fp-WP	1.508	0.557	0.158	0.010	0.011	0.070
F. profunda	Fp-SCS	1.786	0.641	0.154	0.051	0.052	0.048
small *Reticulofenestra*	Ret (<4um)	2.454	0.509	0.848	0.354	0.416	0.141
E. huxleyi	Emi	2.512	0.469	0.853	0.054	0.064	0.135
Gephyocapsa spp.	G spp	2.755	0.502	0.752	0.125	0.147	0.099
G. caribbeanica	Gcar	3.312	0.352	1.873	0.174	0.192	0.171
U. sibogae	Umb	4.060	0.500	1.268	0.416	0.441	0.077
G. oceanica	Geo	4.187	0.517	1.170	0.155	0.178	0.067
P. lacunosa	Pla	4.350	0.617	1.171	0.337	0.338	0.062
Small *Ca. leptoporus*	Cal small	4.605	0.629	3.351	0.172	0.199	0.158
large *Reticulofenestra*	Ret(>4um)	4.988	0.605	2.379	0.534	0.641	0.096
Cy. floridanus	Cyf	5.805	0.963	4.174	0.320	0.336	0.124
(dissolved) *Cy. floridanus*	Cyf -d	6.134	0.727	4.508	0.352	0.417	0.120
Large *Ca. leptoporus*	Cal large	6.370	0.931	3.737	1.053	1.336	0.092
H. carteri	Hel	8.936	0.994	2.541	1.740	2.440	0.032
Co. pelagicus	Cpl	10.640	1.175	10.610	0.950	1.235	0.094

Figure 1. Temporal and spatial distribution of samples. (a) The evolution of studied coccoliths: first occurrence and last occurrence data are from Nannotax3 (http://www.mikrotax.org/Nannotax3/index.html). The blue bars represent ranges of first occurrence and the green bars represent ranges of last occurrence. The blue diamonds represent samples used in this study. (b) Spatial distribution of samples. 1304 means IODP U1304, 3428 means MD12-3428cq, 1433 and 1435 means IODP U1433 and U1435, respectively. 807 means ODP 807 and 21-2 means KX21-2.

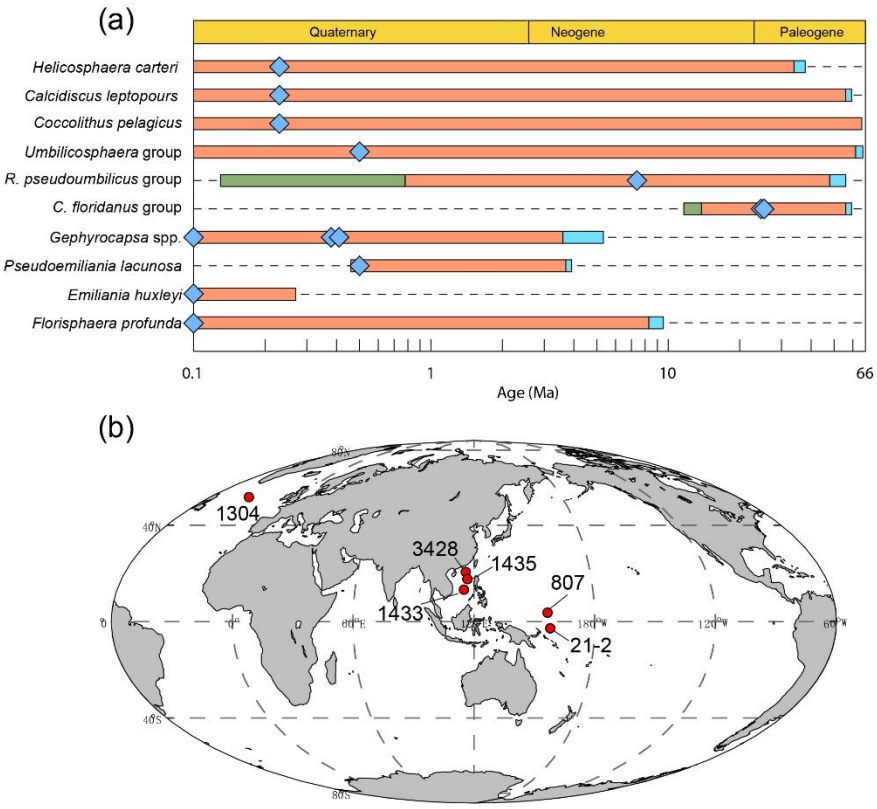

290

291 **Figure 2.** Schematic of settling experiments. V_1 and V_2 are the volumes of the upper and lower

292 cylinders, D is the settled distance. The numbers in circles are same as the number of Steps described in

293 Section 2.2.1.

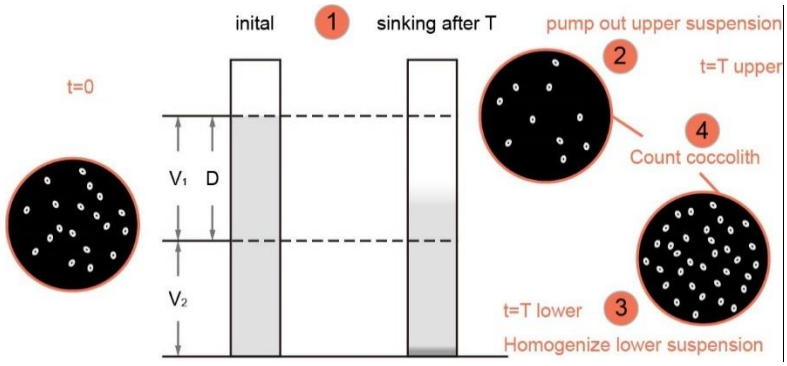

294

Figure 3. The shape parameters of vessels. V_1 and V_2 means the volume of upper suspension and lower suspension, respectively. D means sinking distance. Φ means average inner diameter which is calculated by $2*(V_1/\pi D)^{-2}$.

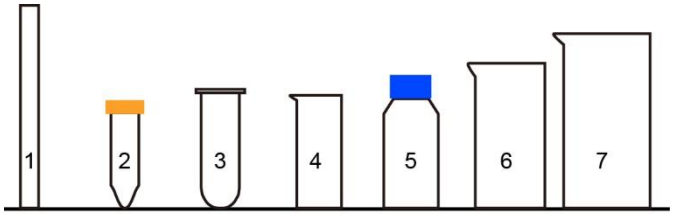

No.	Name	V1	V2	D (cm)	Φ (cm)
1	25 ml comparsion tube	15	10	6.376	1.73
2	50 ml centrifuge tube	30	20	5.480	2.64
3	100 ml centrifuge tube	50	30	4.854	3.62
4	100 ml beaker	40	40	2.834	4.24
5	100 ml reagent bottle	40	40	1.900	5.18
6	250 ml beaker	150	100	4.400	6.59
7	500 ml beaker	300	200	5.700	8.19

Figure 4. Sinking velocities of *G. oceanica* in the core KX-21-2 measured in different vessels. (a) The calibrated separation ratios measured in different vessels. Error bars show 95% confidence level of calibrated separation ratio. (b-d) The relationship between sinking velocity and different vessel shape parameters. Error bars represent 95% confidence level of sinking velocity in each vessel and the shade area represents 95% confidence level of sinking velocity considering all data points.

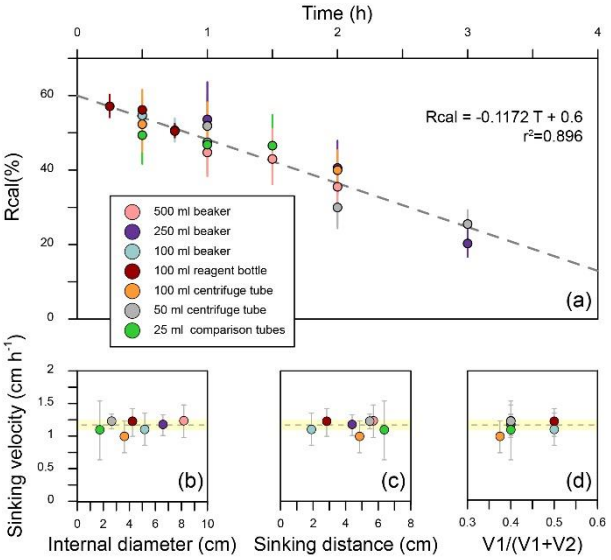

Figure 5. The calculated separation ratio (Rcal) vs sinking duration. Fp-WP means *F. profunda* in the West Pacific. Fp-SCS means *F. profunda* in the South China Sea. Emi means *E. huxleyi*. Gspp means small *Geophyocapsa*. Geo means *G. oceanica*. Gcarb means *G. caribbeanica*. Ret<4 means small *Reticulofenestra*. Ret>4 means large *Reticuloenestra*. Cyf means *Cyclicargolithus floridanus*. Cy-d means dissolved *Cy. floridanus*. Umb means *U. sibogae*. Pla means *Pseudoemiliania lacunosa*. Hel means *H. carteri*. Cal large means larger *Calicidiscus leptoporus*. Cal small means small *Ca. leptoporus*. Cpl means *Co. pelagicus*.

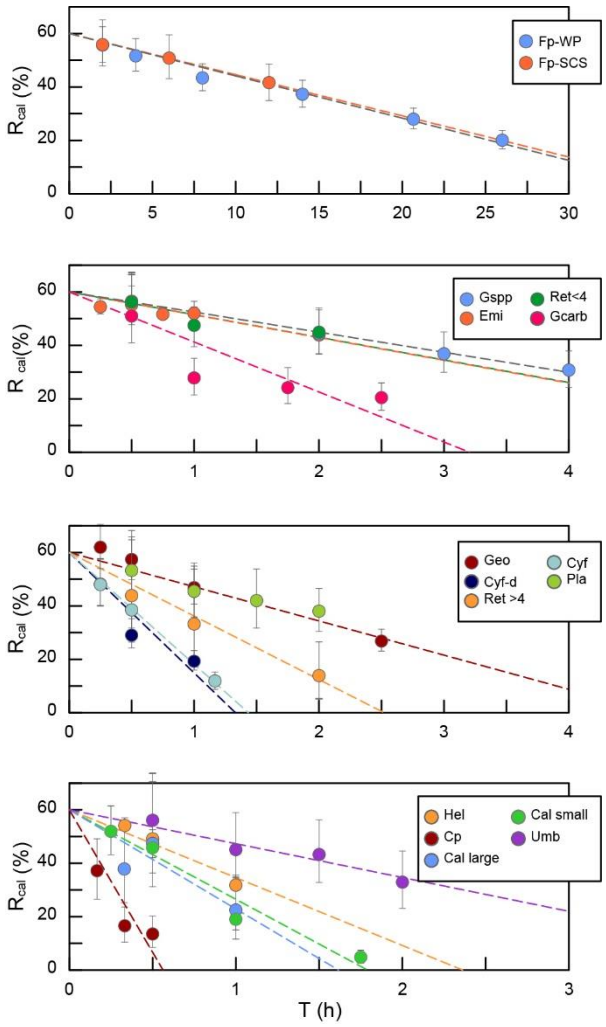

Figure 6. Coccolith sinking velocities and coccolith shape factors. (a-b) Sinking velocities and mean distal shield length. The horizontal error bars represent one standard deviation of coccolith length and the vertical ones represent 95% confidence level of measured sinking velocities. The blue, green and red lines represent sinking velocity of calcite sphere objects, coccolith sinking velocities estimated by Bolton et al. (2012) and this study, respectively. (c) The ratio of measured speed and speed calculated by Stokes' Law. (d) Coccolith short axis length (SAL) and long axis length (LAL) ratio against shape-velocity factor k_v. Box shows median value and upper/lower quartiles, whiskers show maximum and minimum values, outliers larger than 1.5 of the interquartile range are shown as red crosses. The SAL against LAL plot was shown in Figure C3. The short names of coccoliths can be found in Table 2.

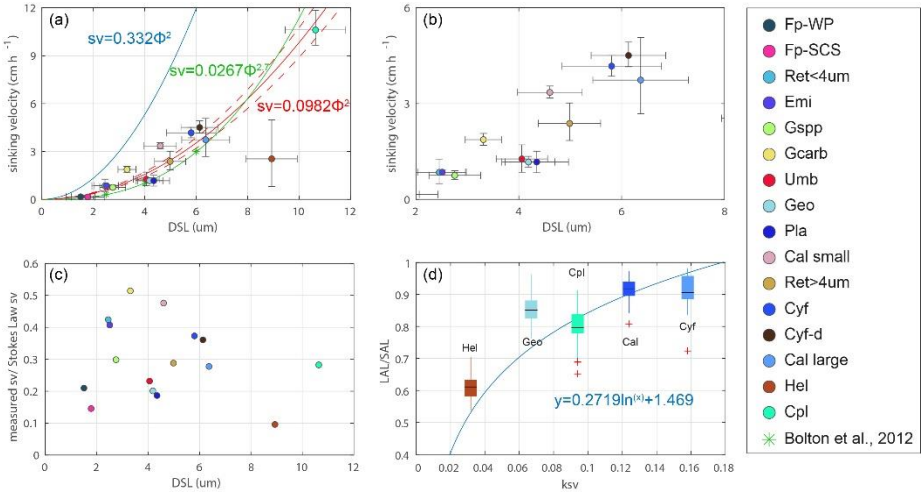

Figure 7. The selection of separation velocities: the sinking velocities of three main coccolith species in sample from core KX21-2 were calculated by the length distribution and velocity factors in Table 2. The yellow dots represent sinking velocities of coccoliths with mean length. The edge of boxes show the sinking velocities of coccolith within one standard deviation of length (±1σ) and the whiskers mark the sinking velocities of coccolith within two standard deviation of length (±2σ).

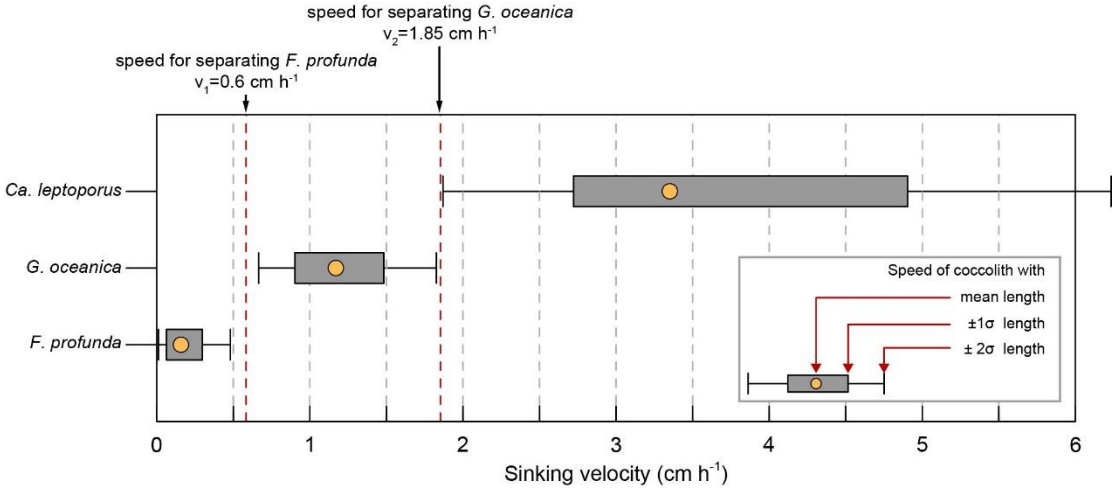

References

Bach, L.T., Riebesell, U., Sett, S., Febiri, S., Rzepka, P., Schulz, K.G., 2012. An approach for particle sinking velocity measurements in the 3-400 mum size range and considerations on the effect of temperature on sinking rates. Mar Biol 159, 1853-1864, doi:10.1007/s00227-012-1945-2.

Barnea, E., Mizrahi, J., 1973. A generalized approach to the fluid dynamics of particulate systems: Part 1. General correlation for fluidization and sedimentation in solid multiparticle systems. The Chemical Engineering Journal 5, 171-189, doi:10.1016/0300-9467(73)80008-5.

Baumann, K.-H., 2004. Importance of size measurements for coccolith carbonate flux estimates. Micropaleontology, 35-43.

Beaufort, L., Lancelot, Y., Camberlin, P., Cayre, O., Vincent, E., Bassinot, F., Labeyrie, L., 1997. Insolation cycles as a major control of equatorial Indian Ocean primary production. Science 278, 1451-1454, doi:10.1126/science.278.5342.1451.

Beltran, C., de Rafélis, M., Minoletti, F., Renard, M., Sicre, M.A., Ezat, U., 2007. Coccolith $\delta^{18}O$ and alkenone records in middle Pliocene orbitally controlled deposits: High-frequency temperature and salinity variations of sea surface water. Geochemistry, Geophysics, Geosystems 8, Q05003, doi:10.1029/2006GC001483.

Bolton, C.T., Hernandez-Sanchez, M.T., Fuertes, M.A., Gonzalez-Lemos, S., Abrevaya, L., Mendez-Vicente, A., Flores, J.A., Probert, I., Giosan, L., Johnson, J., Stoll, H.M., 2016. Decrease in coccolithophore calcification and CO2 since the middle Miocene. Nat Commun 7, 10284, doi:10.1038/ncomms10284.

Bolton, C.T., Stoll, H.M., 2013. Late Miocene threshold response of marine algae to carbon dioxide limitation. Nature 500, 558-562, doi:10.1038/nature12448.

Bolton, C.T., Stoll, H.M., Mendez-Vicente, A., 2012. Vital effects in coccolith calcite: Cenozoic climate-pCO2drove the diversity of carbon acquisition strategies in coccolithophores, Paleoceanography 27, doi:10.1029/2012pa002339.

Bordiga, M., Bartol, M., Henderiks, J., 2015. Absolute nannofossil abundance estimates: Quantifying the pros and cons of different techniques. Revue de micropaléontologie 58,

155-165 doi:10.1016/j.revmic.2015.05.002.

Candelier, Y., Minoletti, F., Probert, I., Hermoso, M., 2013. Temperature dependence of oxygen isotope fractionation in coccolith calcite: A culture and core top calibration of the genus Calcidiscus. Geochimica et Cosmochimica Acta 100, 264-281, doi:10.1016/j.gca.2012.09.040.

Hermoso, M., Candelier, Y., Browning, T.J., Minoletti, F., 2015. Environmental control of the isotopic composition of subfossil coccolith calcite: Are laboratory culture data transferable to the natural environment? GeoResJ 7, 35-42, doi:10.1016/j.grj.2015.05.002.

Hermoso, M., Chan, I.Z.X., McClelland, H.L.O., Heureux, A.M.C., Rickaby, R.E.M., 2016. Vanishing coccolith vital effects with alleviated carbon limitation. Biogeosciences 13, 301-312, doi:10.5194/bg-13-301-2016.

Jin, X., Liu, C., Poulton, A.J., Dai, M., Guo, X., 2016. Coccolithophore responses to environmental variability in the South China Sea: species composition and calcite content. Biogeosciences 13, 4843-4861, doi: 10.5194/bg-13-4843-2016.

Kell, G.S., 1975. Density, thermal expansivity, and compressibility of liquid water from 0. deg. to 150. deg.. correlations and tables for atmospheric pressure and saturation reviewed and expressed on 1968 temperature scale. Journal of Chemical and Engineering Data 20, 97-105.

Kestin, J., Sokolov, M., Wakeham, W.A., 1978. Viscosity of liquid water in the range −8 °C to 150 °C. Journal of Physical and Chemical Reference Data 7, 941-948.

Koch, C., Young, J., 2007. A simple weighing and dilution technique for determining absolute abundances of coccoliths from sediment samples. J. Nannoplankton Res.

McClelland, H.L., Bruggeman, J., Hermoso, M., Rickaby, R.E., 2017. The origin of carbon isotope vital effects in coccolith calcite. Nat Commun 8, 14511, doi:10.1038/ncomms14511.

McClelland, H.L., Barbarin, N., Beaufort, L., Hermoso, M., Ferretti, P., Greaves, M., Rickaby, R.E.M., 2016. Calcification response of a key phytoplankton family to millennial-scale environmental change. Scientific Reports 6, 34263, doi: 10.1038/srep34263.

McNown, John S., and Jamil Malaika. "Effects of particle shape on settling velocity at low

391 Reynolds numbers." Eos, Transactions American Geophysical Union 31.1 (1950): 74-82.
392 Miklasz, K.A., Denny, M.W., 2010. Diatom sinkings speeds: Improved predictions and insight
393 from a modified Stokes' law. Limnology and Oceanography 55, 2513-2525,
394 doi:10.4319/lo.2010.55.6.2513.
395 Minoletti, F., Hermoso, M., Gressier, V., 2009. Separation of sedimentary micron-sized
396 particles for palaeoceanography and calcareous nannoplankton biogeochemistry. Nat.
397 Protocols 4, 14-24, doi:10.1038/nprot.2008.200.
398 Paull, C.K., Thierstein, H.R., 1987. Stable isotopic fractionation among particles in Quaternary
399 coccolith-sized deep-sea sediments. Paleoceanography 2, 423-429,
400 doi:10.1029/PA002i004p00423.
401 Edwards, A.R., 1963. A preparation technique for calcareous nannoplankton.
402 Micropaleontology 9, 103-104.
403 Richardson, J., Zaki, W., 1954. The sedimentation of a suspension of uniform spheres under
404 conditions of viscous flow. Chemical Engineering Science 3, 65-73.
405 Rickaby, R.E.M., Henderiks, J., Young, J.N., 2010. Perturbing phytoplankton: response and
406 isotopic fractionation with changing carbonate chemistry in two coccolithophore species.
407 Clim. Past 6, 771-785, doi:10.5194/cp-6-771-2010.
408 Rousselle, G., Beltran, C., Sicre, M.-A., Raffi, I., De Rafélis, M., 2013. Changes in sea-surface
409 conditions in the Equatorial Pacific during the middle Miocene–Pliocene as inferred from
410 coccolith geochemistry. Earth and Planetary Science Letters 361, 412-421,
411 doi:10.1016/j.epsl.2012.11.003.
412 Sprengel, C., Baumann, K.-H., Henderiks, J., Henrich, R., Neuer, S., 2002. Modern
413 coccolithophore and carbonate sedimentation along a productivity gradient in the Canary
414 Islands region: seasonal export production and surface accumulation rates. Deep Sea
415 Research Part II: Topical Studies in Oceanography 49, 3577-3598 doi: 10.1016/S0967-
416 0645(02)00099-1.
417 Stoll, H.M., 2005. Limited range of interspecific vital effects in coccolith stable isotopic records
418 during the Paleocene-Eocene thermal maximum. Paleoceanography 20,
419 doi:10.1029/2004pa001046.

Stoll, H.M., Rosenthal, Y., Falkowski, P., 2002. Climate proxies from Sr/Ca of coccolith calcite: calibrations from continuous culture of Emiliania huxleyi. Geochimica et Cosmochimica Acta 66, 927-936, doi:10.1016/S0016-7037(01)00836-5.

Stoll, H.M., Ziveri, P., 2002. Separation of monospecific and restricted coccolith assemblages from sediments using differential settling velocity. Marine Micropaleontology 46, 209-221, doi: 10.1016/S0377-8398(02)00040-3.

Xie, H-Y., and D-W. Zhang. "Stokes shape factor and its application in the measurement of spherity of non-spherical particles." Powder Technology 114.1 (2001): 102-105 doi: 10.1016/S0032-5910(00)00269-2.

Young, J.R., Ziveri, P., 2000. Calculation of coccolith volume and it use in calibration of carbonate flux estimates. Deep sea research Part II: Topical studies in oceanography 47, 1679-1700, doi:10.1016/S0967-0645(00)00003-5.

Zhang, H., Liu, C., Jin, X., Shi, J., Zhao, S., Jian, Z., 2016. Dynamics of primary productivity in the northern South China Sea over the past 24,000 years. Geochemistry, Geophysics, Geosystems 17, 4878-4891, doi:10.1002/2016GC006602 .

Ziveri, P., Stoll, H., Probert, I., Klaas, C., Geisen, M., Ganssen, G., Young, J., 2003. Stable isotope 'vital effects' in coccolith calcite. Earth and Planetary Science Letters 210, 137-149, doi:10.1016/S0012-821X(03)00101-8.

Appendix A. Sample selections

Table A1. Sample selections

Measured coccolith	abb.	Region	Core	Section	Epoch	Age model ref.
F. profunda	Fp-SCS	SCS	MD12-3428	0-1 cm	Holocene	Zhang et al., 2016
F. profunda	Fp-WP	W.P.	KX21-2	2-4 cm	Holocene	Liang et al., 2016
E. huxleyi	Emi	SCS	MD12-3428	0-1 cm	Holocene	Zhang et al., 2016
Gephyocapsa spp.	Gspp	W.P.	ODP 807A	1H 5W 102-104	Pleistocene	Jin et al., 2010
G. oceanica	Geo	W.P.	KX21-2	2-4 cm	Holocene	Liang et al., 2016
G. caribbeanica	Gcarb	N.A.	IODP 1304B	7H 5W 69-70	Pleistocene	Channell et al., 2010
small *Reticulofenestra*	Ret<4	SCS	IODP 1433B	28R 2W 30-34	Miocene	Li et al., 2013
large *Reticulofenestra*	Ret>4	SCS	IODP 1433B	28R 2W 30-34	Miocene	Li et al., 2013
Cyclicargolithus floridanus	Cyf	SCS	IODP 1435A	6R 3W 25-29	Oligocene	Li et al., 2013
Cyclicargolithus floridanus	Cyf-d	SCS	IODP 1435A	8R 1W 27-31	Oligocene	Li et al., 2013
Umbilicosphaera sibogae	Umb	W.P.	ODP 807A	3H 5W 92-94	Pleistocene	Jin et al., 2010
Pseudoemiliania lacunosa	Pla	W.P.	ODP 807A	3H 5W 92-94	Pleistocene	Jin et al., 2010
Helicosphaera carteri	Hel	W.P.	ODP 807A	3H 5W 92-94	Pleistocene	Jin et al., 2010
large *Calcidiscus leptoporus*	Cal large	W.P.	ODP 807A	3H 5W 92-94	Pleistocene	Jin et al., 2010
small *Calcidiscus leptoporus*	Cal small	N.A.	IODP 1304B	7H 5W 69-70	Pleistocene	Channell et al., 2010
Coccolithus pelagicus	Cpl	N.A.	IODP 1304B	7H 5W 69-70	Pleistocene	Channell et al., 2010

References:

Channell, J., Sato, T., Kanamatsu, T., Stein, R., Alvarez Zarikian, C., 2010. Expedition 303/306 synthesis: North Atlantic climate. Channell, JET, Kanamatsu, T., Sato, T., Stein, R., Alvarez Zarikian, CA, Malone, MJ, and the Expedition 303, 306.

Jin, H., Jian, Z., Cheng, X., Guo, J., 2011. Early Pleistocene formation of the asymmetric east-west pattern of upper water structure in the equatorial Pacific Ocean. Chinese Science Bulletin 56, 2251-2257.

Li, C.-F., Lin, J., Kulhanek, D.K., 2013. South China Sea tectonics: Opening of the South China Sea and its implications for southeastAsian tectonics, climates, and deep mantle processes since the late Mesozoic. IODP Sci. Prosp 349.

Liang, D., Liu, C., 2016. Variations and controlling factors of the coccolith weight in the Western Pacific Warm Pool over the last 200 ka. Journal of Ocean University of China 15, 456-464.

Zhang, H., Liu, C., Jin, X., Shi, J., Zhao, S., Jian, Z., 2016. Dynamics of primary productivity in the northern South China Sea over the past 24,000 years. Geochemistry, Geophysics, Geosystems 17, 4878-4891.

Appendix B. Coccolith images under circular polarized light

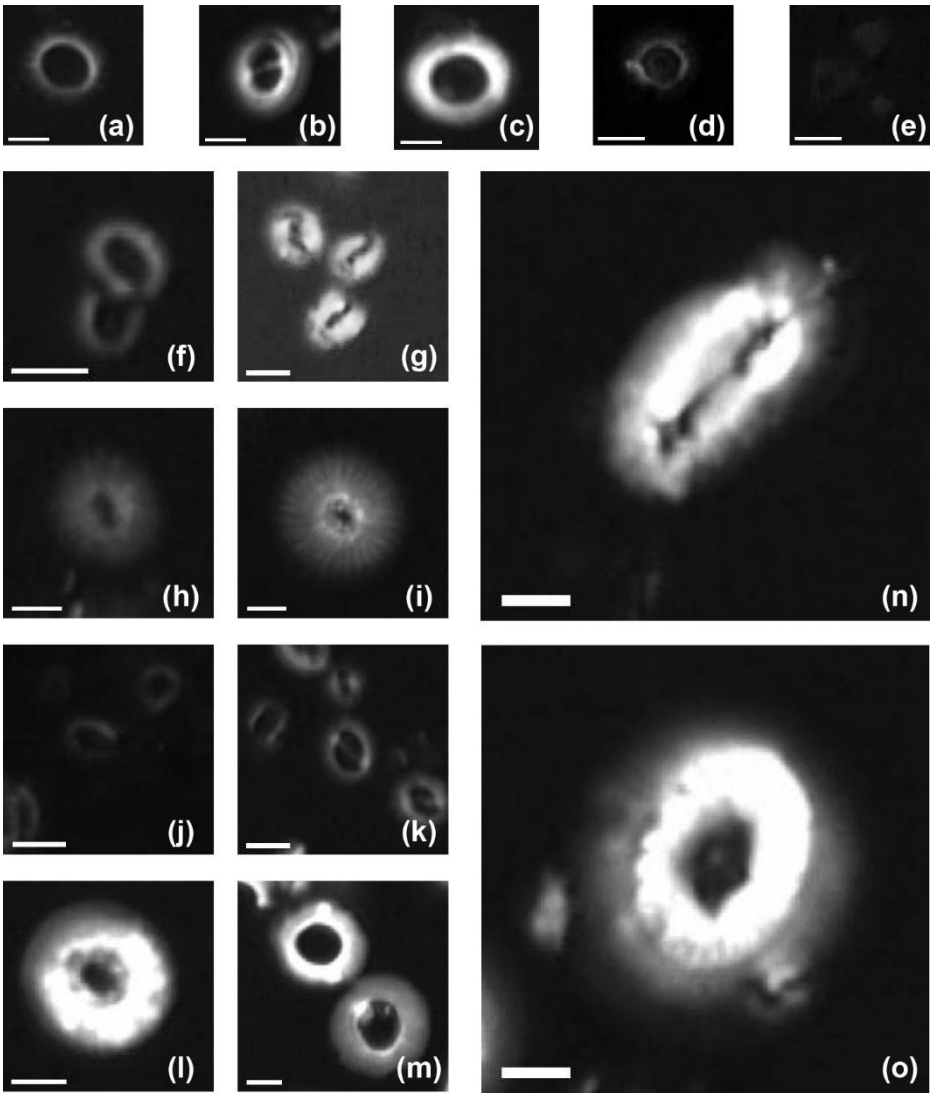

Plate B1. Imaged of measured coccolith in this study: (a) *Pseudoemiliania lacinosa* in the core ODP 807; (b) *Gephyrocapsa oceanica* in the core KX21-2; (c) *Reticulofenestra* spp. (large) in the core IODP U1433B; (d) *Umbilicosphaera sibogae* in the core ODP 807; (e) *Florispharea profunda* in the core KX21-2; (f) *Reticulofenestra* spp. (small) in the core IODP U1433B; (g) *Gephyrocapsa caribbeanica* in the core IODP U1304B; (h) small *Calcidiscus leptoporus* in the core IODP U1304B; (i) large *Calcidiscus leptoporus* in the core ODP 807A; (j) *Emiliania huxleyi* in the surface sediment in the South China Sea; (k) *Gephyrocapsa* spp. in the core ODP 807; (l) *Cyclicargolithus floridanus* in the core IODP U1435A and (m) dissolved *Cyclicargolithus floridanus* in the same core; (n) *Helicosphaera carteri* in the core ODP 807A; (o) *Coccolithus pelagicus* in the core IODP U1304B. White bars represent a length of 2 μm.

Appendix C. The length distribution of coccoliths

To measure the distal shield length of coccoliths, pictures were taken at a magnification of 1250x under circular polarized light. The coccolith lengths were measured by using the image analysis software, ImageJ. More than 5 pictures were taken and more than 50 (usually more than 100) coccolith specimens were measured. The length distributions of coccoliths measured in our experiments were shown in the Figure C1.

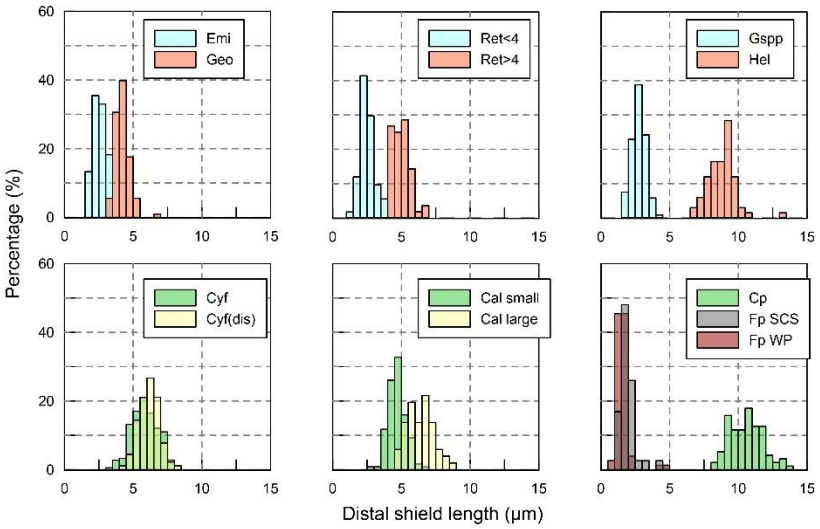

Figure C1. Size distribution of coccolith measured in the present study. The shorten names of coccolith follow Table A1.

The classification of coccoliths by length was supported by mixture analysis in PAST (Hammer et al., 2001), such as *Reticulofenestra* spp. and *Gephyrocapsa* spp. *Reticulofenestra* spp. in the Miocene were classified into two groups, Ret. (<4 μm) and Ret. (>4 μm). The traditional classification of *Reticulofenestra* spp. is <3 μm, 3-5 μm and 5-7 μm didn't pass the normal distribution test. Hence, in this study the *Reticulofenestra* spp. are divided at 4 μm (Figure C2). *Gephyrocapsa* spp. were classified by the shape of coccoliths into small *Gephyrocapsa* (central area opening and length <3.5 μm), *G. oceanica* (central area opening and length >3.5μm) and *G. caribbeanica* (closed central area) by the length and central area.

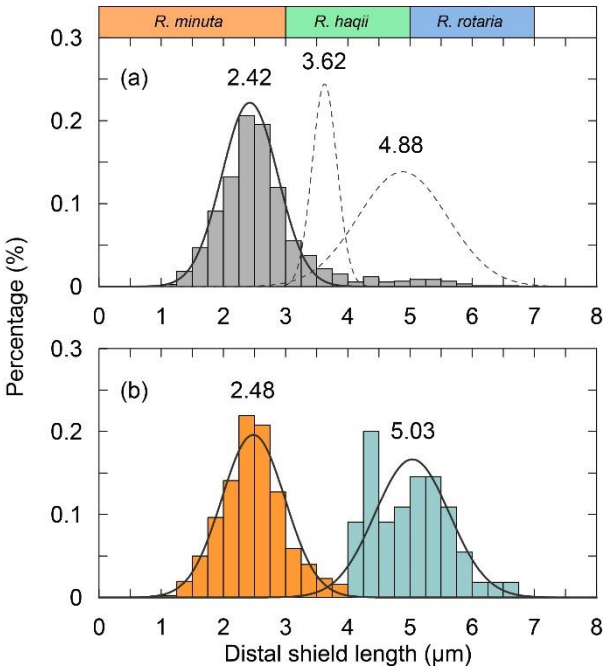

Figure C2. The classical classification of *Reticulofenestra* spp. (a) and the classification used in our study (b). The curves represent the normal distribution fits of different coccolith groups and the dish curve marks that the goodness of fit is below 0.2.

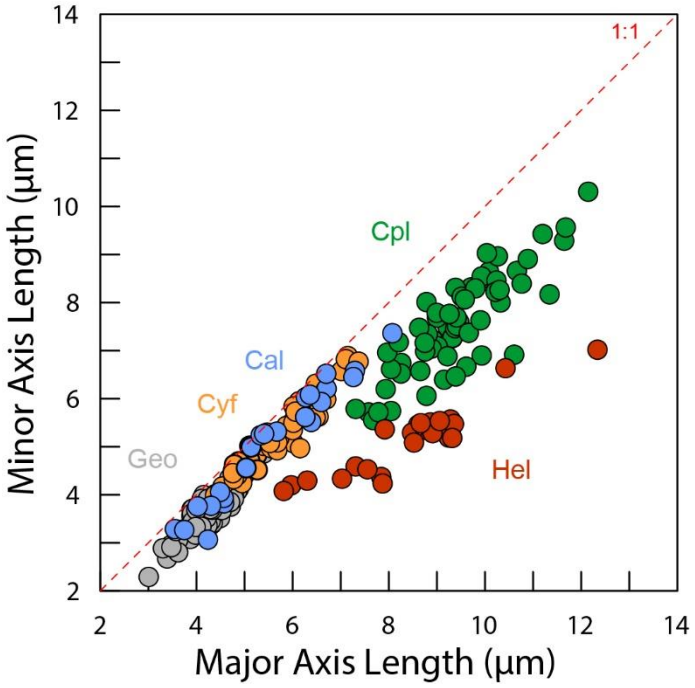

Figure C3. The short axis and long axis length distribution of coccoliths in Figure 6d.

Reference.

493 Hammer, Ø., Harper, D., Ryan, P., 2001. Paleontological Statistics Software: Package for
494 Education and Data Analysis. Palaeontologia Electronica.

Appendix D. Coccolith movement in gravity settling

In this part, the derivation of equation will be explained in detail including proofs of several assumptions mentioned in the methods part.

When the well mixed sediment begins to sink, the decrease of coccoliths number in the upper suspension (N_u) can be described as following equation:

$$\frac{dN_u}{dT} = -\frac{N_{u(t=0)}}{D} \times v \tag{D-1}$$

where the D is the length of upper suspension and $N_{u(t=0)}$ /D is the initial number of coccolith in cross-section with a unit thickness, v is the sinking velocity of coccolith.

Do integration for the equation D-1, we can get the variation of coccolith number in the upper column over time:

$$N_u = N_{u(t=0)} - \frac{N_{u(t=0)}}{D} \times v \times T \tag{D-2}$$

where T is settling time. After a period of time (T), we pump out the upper suspension. Here we define the number of coccoliths in the upper supernatant dividing the total coccoliths number in the tube (N_t) as separation ratio (R), which represents the percentage of total coccoliths removed in one separation. R can be expressed by

$$R = \frac{Nu}{Nt} \tag{D-3}$$

Assuming all coccoliths are uniformly distributed in the suspension at the beginning of settling, $N_{u(t=0)}$ has relationship with N_t as follow:

$$\frac{Nu(t=0)}{Nt} = \frac{V_1}{V_1+V_2} \tag{D-4}$$

where V_1 is the volume of upper suspensions and V_2 is the volume of lower suspensions.

Combining the equation D-1, D-2, D-3 and D-4, we obtain the relationship between separation ratio, R, and sinking velocity, v, as follow:

$$R = \frac{N_u}{N_t} = \frac{N_{u(t=0)} - \frac{N_{u(t=0)}}{D} \times v \times T}{N_t} = \frac{V_1 - \frac{V_1}{D} \times v \times T}{V_1+V_2} \tag{D-5}$$

If we plot the R and T on a figure, the slope of the line is a function of V_1, V_2, D and v. Since the V_1, V_2, D are known parameters, we say the slope of R-T is a function of v, which is exactly what we want.

Comparison tubes used in our experiments have the same V_1 and V_2 but different D. Other vessels used in other experiments have different V_1, V_2 and D. So we should adjust the raw separation ratio

to calibrated separation ratio (R_{cal}), which represents the separation ratio made in a standard vessel with V_{1std}=15 ml, V_{2std}=10 ml and D_{std}=6 cm. This step can be described by equation D-6:

$$R_{cal} = \frac{[R\times(V_1+V_1)-V_1]\times D\times V_{1std}}{(D_{std}\times V_1+V_{1std})\times(V_{1std}+V_{2std})} \quad \text{(D-6)}$$

After calibrated, the slope of R_{cal}-T (k) has relationship with v as following equation:

$$v = -\frac{D_{std}\times(V_{1std}+V_{2std})}{V_{1std}} \times k = -10 \times k \quad \text{(D-7)}$$

where k is the slope of R_{cal} against T from regression and other parameters are as described above. Hence, the sinking velocity of different coccoliths can be achieved by measuring the variations of R_{cal} over time.

The coccoliths' lengths in the sediment have some varations. So what we measured is actually the bulk settling velocity of whole coccolith population. We also offer a test for the assumption that the average sinking velocity of all coccoliths can be treated as the sinking velocity of coccoliths with the average length. Here we used the data of *G. oceanica*. A normal distribution was fitted to the measured length distribution (Figure D1-a). We generated 100000 coccolith following the normal distribution and let these coccolith evenly distributing in the comparison tube at the initial and then set them sinking without collisions with each other. The sinking velocities of different size coccoliths were calculated by the velocity-shape parameter 'k_v' as described in discussion part. We modeled the coccoliths sinking process and computed the separation ratio (red dash line in Figure D1-b), coccolith length (red dash line in Figure D1-c) and instant sinking velocities (orange dots in Figure D1-d) at different time sections.

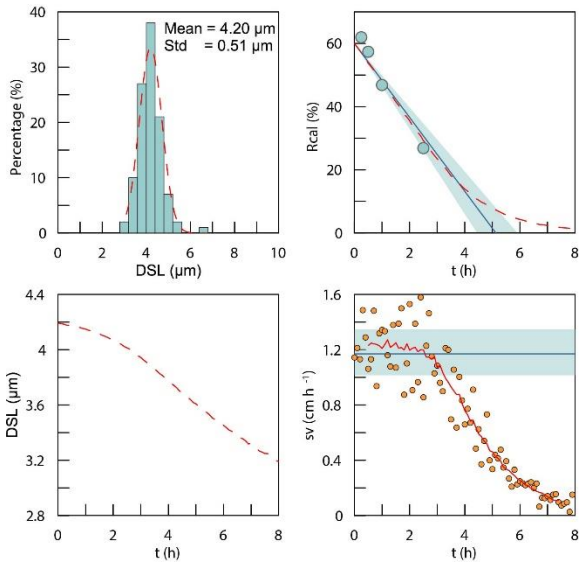

Figure D1. The simulations of coccoliths settling with different lengths: (a) the length distribution of coccoliths. The green bars represent measured data and red dash line represents the best fit for normal distribution. (b) The calibrated separation ratio: the green dots are measured data in our settling experiments, the blue line and shade area represent the calculated sinking velocity based on R_{cal} measurement and the red dash line represents results obtained from simulations. (c) The average length of removed coccolith in simulations; (d) the modeling sinking velocities of coccoliths: the orange dots are instant sinking velocity calculated from derivation of R_{cal}, the red dash line is weighted average for the instant sinking velocity. Blue line represents the average sinking velocity we measured and the green shade area represents 95% confidence level of the measured velocity.

For *G. oceanica* experiments, the instant sinking velocity would not change significantly until settling for more 3 hours. That means for all R_{cal} larger than 15% are safe for liner regressions. The minimum safe number of R_{cal} will descend with the drop of dispersion degree of coccolith length distribution. Hence our assumption for average sinking velocity and the use of liner regression are proved to be reasonable.

Appendix E. Statistical and error analyses

The errors of measured separation ratio (R) and calculated sinking velocity (v) are mainly caused by counting coccolith, the error of which fellows the Poisson distribution. To detect the influence of counting number on the result error, the error of separation ratio was simulated by 5000 times Monte Carlo calculations with assumptions that 'V_1:V_2=15:10' and 'n_1=n_2' (Figure E1). The result shows that the number of coccolith counted in the upper column draws more influence on the relative error ($|R-R_{95CL}|/R$). That means more coccolith in the upper suspension should be counted to make results more accurate. The slope of R_{cal}-T was calculated by liner fitting with the intercept fixed on $V_1/(V_1+V_2)$. The input R_{cal} were generated from measured values considering the error of coccolith counting. The regressions of R_{cal}-T were repeated by 5000 times regressions in the software Matlab and the error of sinking velocity, v, was source from the distribution slope of R_{cal}-T in Monte Carlo process.

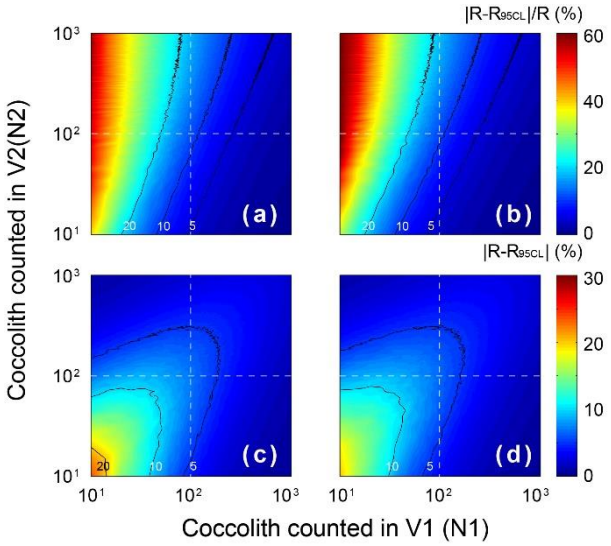

Figure E1. The error distribution with different N_1 and N_2 (ranging from 1 to 1000) simulated 5000 times by the Matlab with assumptions that the error distributions of N_1 and N_2 fellow Poisson distribution. The calculation of R follows equation 2-5, and here we assume numbers of FOV are equal (n_1=n_2). Counter lines mark values equal to 5, 10 and 20. (a) and (c) represent the lower 95% confidence level and (b) and (d) represent upper 95% confidence level. (a) and (b) the relative error of R and (c) and (d) represent the absolute error of R.